communications materials

Article

https://doi.org/10.1038/s43246-024-00633-x

High-temperature Brown-Zak oscillations in graphene/hBN moiré field effect transistor fabricated using molecular beam epitaxy

Oleg Makarovsky[1] ✉, Richard J. A. Hill[1], Tin S. Cheng[1], Alex Summerfield[1], Takeshi Taniguchi[2], Kenji Watanabe[2], Christopher J. Mellor[1], Amalia Patanè[1], Laurence Eaves[1], Sergei V. Novikov[1] & Peter H. Beton[1]

Graphene placed on hexagonal boron nitride (hBN) has received significant interest due to its excellent electrical performance and physics phenomena, such as superlattice Dirac points. Direct molecular beam epitaxy growth of graphene on hBN offers an alternative fabrication route for hBN/graphene devices. Here, we investigate the electronic transport of moiré field effect transistors (FETs) in which the conducting channel is monolayer graphene grown on hexagonal boron nitride by high temperature molecular beam epitaxy (HT-MBE). Alignment between hBN and HT-MBE graphene crystal lattices gives rise to a moiré-fringed hexagonal superlattice pattern. Its electronic band structure takes the form of a "Hofstadter butterfly". When a strong magnetic field B is applied perpendicular to the graphene layer, the electrical conductance displays magneto-oscillations, periodic in B^{-1}, over a wide range of gate voltages and temperatures up to 350 K. We attribute this behaviour to the quantisation of electronic charge and magnetic flux within each unit cell of the superlattice, which gives rise to so-called Brown-Zak oscillations, previously reported only in high-mobility exfoliated graphene. Thus, this HT-MBE graphene/hBN heterostructure provides a platform for observation of room temperature quantum effects and device applications.

Single layer graphene[1] has unique electronic properties, including record high room temperature carrier mobility[2–4], for fundamental studies of quantum phenomena in novel quantum transport devices, such as moiré superlattices[5–7] and moiré field effect transistors (FETs)[8]. A large number of growth and fabrication techniques have been developed in the last 20 years to improve graphene quality and scalability for applications in electronic devices. At present, the best performance is achieved with exfoliated graphene encapsulated by another remarkable material, hexagonal boron nitride, hBN[9]. FETs fabricated from hBN-encapsulated graphene using the exfoliation-stamping technique exhibit record high carrier mobility, reaching 500,000 cm^2/Vs[3]. However, attempts to adapt hBN/graphene FET technology for large scale fabrication and epitaxial growth have so far met with only limited success. Graphene/hBN FETs fabricated using chemical vapour deposition (CVD) either require manual hBN encapsulation of individual flakes[4] or demonstrate rather moderate mobility of about 10,000 cm^2/Vs[10]. High temperature molecular beam epitaxy (HT-MBE) growth of single layer graphene directly on an hBN substrate[11–13] provides an alternative route for making hBN/graphene devices. Despite significant interest in the growth of MBE graphene and hBN[14–16], we believe that this is the first report on the transport properties of an HT-MBE hBN/graphene FET device.

An opportunity to combine 2D materials in a "LEGO building-block" way has led to a new class of functional materials, van der Waals (vdW) heterostructures[17–19]. One of the simplest vdW heterostructure consists of a layer of exfoliated graphene placed on the atomically flat surface of an hBN crystal. These two materials have lattice constants that differ by only ~1.8%. When their crystalline axes are carefully aligned to within an angle of ~1°, atomic force microscopy (AFM) reveals a hexagonal moiré pattern on the surface of the graphene layer with a period of typically ~14 nm for aligned, unstrained graphene[20,21]. This periodic pattern generates a superlattice

[1]School of Physics and Astronomy, University of Nottingham, Nottingham, NG7 2RD, UK. [2]The National Institute for Materials Science, Advances Materials Laboratory, 1-1 Namiki, Tsukuba, Ibraki, 305-0044, Japan. ✉e-mail: oleg.makarovsky@nottingham.ac.uk

potential landscape in the graphene layer, which significantly changes its electronic band structure[5,6,20,21].

In an earlier article, we reported that moiré-fringed superlattices with periodicities greater than 14 nm can be formed when graphene is grown by HT-MBE on exfoliated hBN crystals with excellent alignment of the crystal lattices[11]. In some cases, at substrate temperatures above 1600 °C, the pattern is found to diverge towards "infinity", indicating a lattice matching condition between the graphene and hBN[12], which has not been achieved using other growth or processing techniques. Raman spectroscopy measurements on these heterostructures reveal a significant splitting and shifting of the G and 2D peaks of graphene, which confirm that the moiré fringing arises from the presence of large strains of up to ~1.8% for the case of lattice-matched graphene. The large moiré pattern resulting from these strains is an intrinsic feature of graphene grown on hBN by MBE at these temperatures; it is not observed in graphene grown on hBN by CVD. Conductive AFM measurements have also revealed moiré-modulated current through the hBN tunnel barriers[13].

Results

Here we investigate the electrical properties of a planar FET based on a HT-MBE-graphene-hBN heterostructure and mounted on the oxidised surface of a silicon substrate. By applying a gate voltage, it is possible to change the polarity and sheet density of the carriers and measure carrier concentration and mobility. We find that the very low ($<10^{11}$ cm^{-2}) doping level produced by unintentional impurities in our devices is similar to that reported for high-quality hBN/graphene heterostructures produced by exfoliation[2,3]. However, the carrier mobility in our devices is temperature-independent and much lower (about 1000 cm^2/Vs) than in exfoliated graphene. This suggests a different type of dominant scattering mechanism in the HT-MBE-grown hBN/graphene heterostructures. We also investigate the effect of an applied magnetic field, B, on the electrical properties of the devices. We observe a large linear magnetoresistance upon which are superimposed magneto-oscillations, periodic in $1/B$. We attribute these magneto-oscillations to the formation of Brown-Zak minibands when a unit cell of the superlattice is threaded by a unit fraction of a magnetic flux quantum, $1/p$, where p is an integer[22,23].

Our MBE graphene layers are grown at high substrate temperatures (1500 °C) on hBN flakes. Details of the layer growth and device fabrication processes are given in the *Methods* section. Schematic diagrams of the graphene-hBN FET with a bias voltage, V_b, and a gate voltage, V_g, applied between the graphene channel and the boron-doped p-Si substrate and its transfer characteristic at $T = 273$ K are shown in Fig. 1a, b. Figure 1c shows the Raman spectrum of HT-MBE graphene layer with hBN, G, 2D and D_{ag} peaks discussed below. Figure 1d, e show optical and AFM images of the centre of the device, following fabrication together with the contact electrodes and etched MBE graphene surface. Figure 1f presents a typical tapping mode (AC-mode) AFM image of a monolayer of graphene on hBN grown under these conditions, prior to flake transfer and device fabrication. It reveals a moiré pattern with a periodicity, a, of ~14 nm.

The resistance maximum at $V_g = +1.1$ V in Fig. 1c indicates that the polarity of the ungated graphene layer is weakly p-type, with a hole concentration, $p = 8.2 \times 10^{10}$ cm^{-2} at $V_g = 0$. The very small hysteresis of $R(V_g)$ measured at different directions of the V_g-sweep (black arrows in Fig. 1c) can be attributed to the high purity (absence of charge traps) in this HT-MBE graphene. A broader satellite peak in $R(V_g)$ occurs on the hole branch of the plot at $V_g \sim -40$ V.

This additional feature has been investigated intensively in moiré-fringed superlattices made from exfoliated graphene crystallographically-

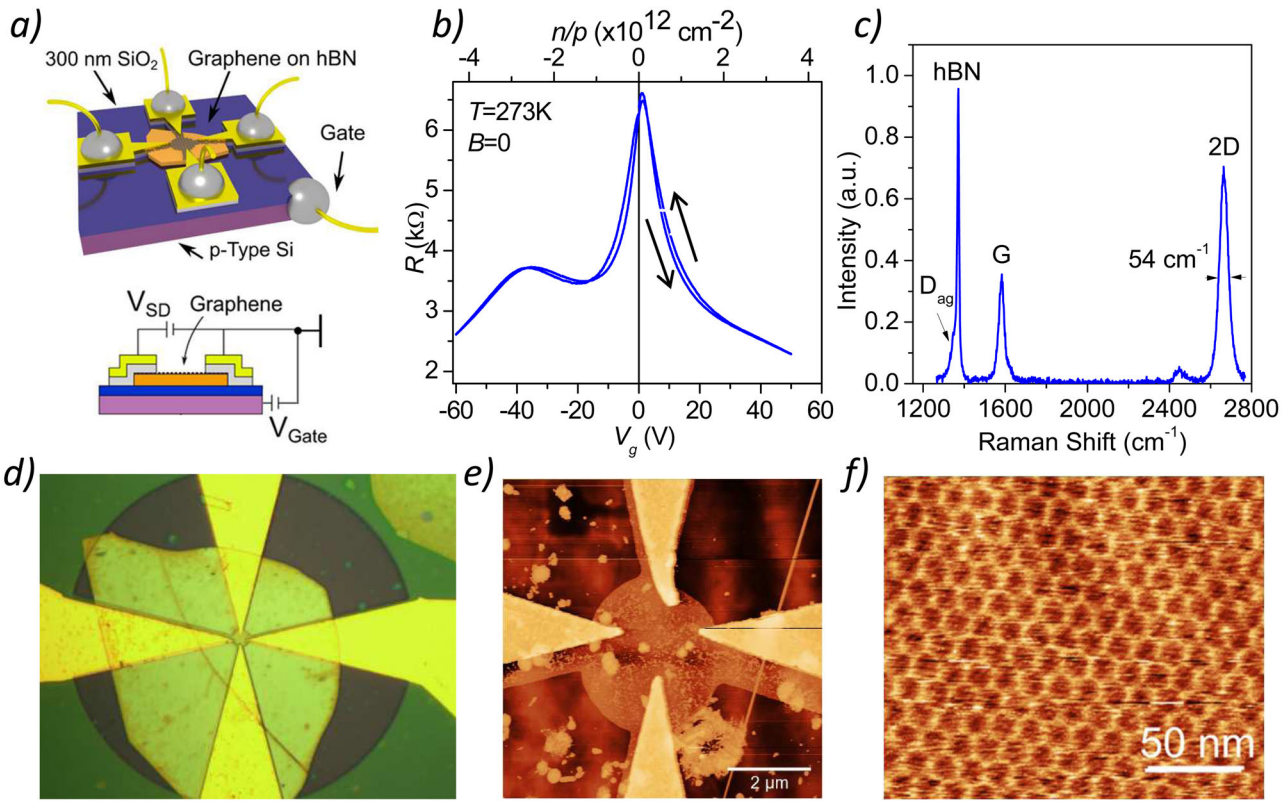

Fig. 1 | HT-MBE graphene FET. a Schematic and connection diagrams of the HT-MBE graphene FET used in the electrical measurement of the transport properties. **b** Raman spectrum of HT-MBE graphene. **c** Resistance of MBE-graphene FET at $T = 273$ K and $B = 0$ as a function of gate voltage V_g. Black arrows indicate directions of the V_g-sweep. **d** Optical image of the region in the main image showing the hBN flake (green) and Au/Ti contacts (gold). **e** AFM image of the centre of the graphene device following fabrication. **f** AC mode AFM image of the pristine graphene surface following HT-MBE growth prior to device fabrication showing a 14 nm period superlattice with the underlying hBN substrate.

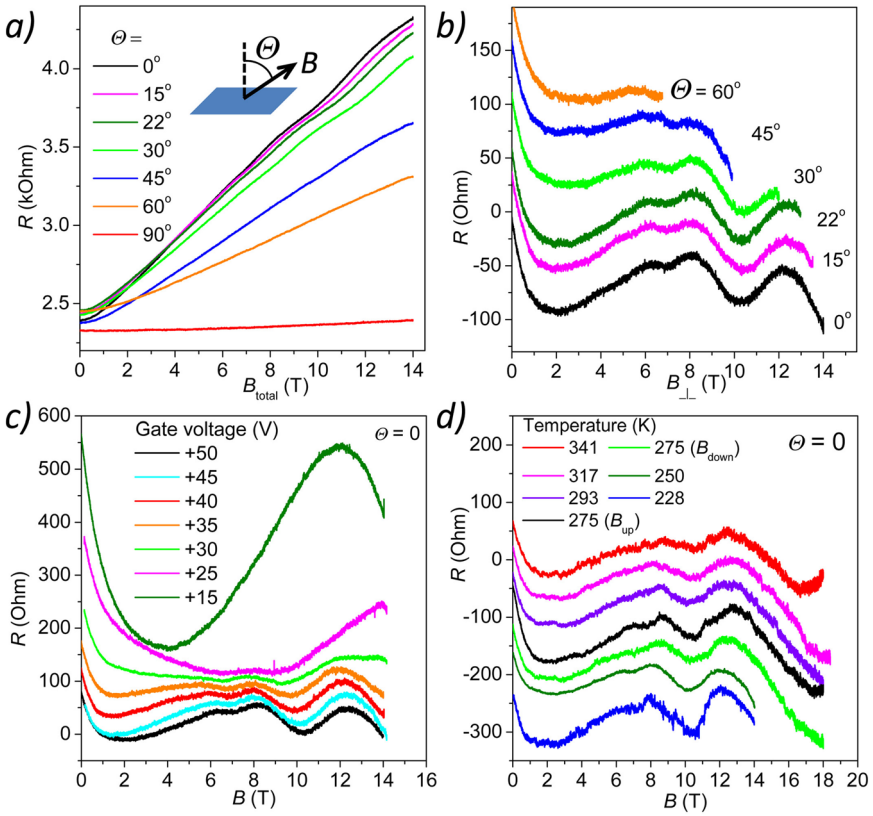

Fig. 2 | Magnetoresistance as a function of temperature, gate voltage and field orientation. **a** Two-terminal residual magnetoresistance of the MBE graphene device at $V_g = +50$ V and $T = 273$ K as a function of the tilt angle, Θ, between the perpendicular to the graphene plane and the applied magnetic field, as shown in the inset. **b** Same data plotted as a function of B component perpendicular to the graphene plane ($B_\perp$) after subtraction of the linear ($R \sim B$) magnetoresistance background. **c** Gate-voltage dependence of magneto-oscillations at $T = 273$ K. **d** Temperature dependence above 228 K of magneto-oscillations up to 18 T at $V_g = +50$ V. B_{up} and B_{down} curves at $T = 275$ K were obtained while sweeping to higher and lower magnetic field, respectively.

aligned on hBN substrates. It is due to the formation of second-generation Dirac points in the valence band produced by the superlattice potential[5,6]. Using a linear fitting of electrical conductivity $\sigma(V_g)$[24], we estimate the room temperature electron and hole mobilities to be $\mu_e = 1300$ cm^2/Vs and $\mu_h = 840$ cm^2/Vs at $T = 273$ K. They have a very weak (<30%) temperature dependence over a wide temperature range 2 K < T < 300 K, see Supplementary Note 1.

The electrical resistance of the device was measured by passing a constant current of $I = 10$ μA through the graphene channel, first in the absence of an applied magnetic field and then in magnetic fields of up to 18 T applied at different tilt angles Θ, to the normal of the graphene sheet. Figure 2a shows the two-terminal magnetoresistance of the device, $R(B)$, at $V_g = +50$ V and at $T = 273$ K, up to fields of 14 T with $\boldsymbol{B}$ oriented at different angles Θ. The large and approximately linear magnetoresistance for Θ = 0 decreases as cos(Θ) when the tilt angle is increased. Inspection of the $R(B)$ curves indicates the presence of magneto-oscillations, which are periodic in $1/B$ and are superimposed upon the large monotonic increase of $R(B)$. The oscillations are shown more clearly in Fig. 2b, in which a linear ($R \sim B$) term is subtracted from the $R(B\cos(\Theta))$ plots. These measurements demonstrate that the period of the magneto-oscillations depends only on the perpendicular component of $\boldsymbol{B}$, $B_\perp = B\cos(\Theta)$, confirming that they arise from the two-dimensional electron system. These oscillations are observed over a wide range of the applied gate voltages (Fig. 2c) and high temperatures $T > 300$ K (Fig. 2d).

Figure 3a, b show the magnetoresistance of the device at $T = 210$ K and $T = 2$ K respectively, at Θ = 0, and different applied gate voltages. At low temperature the structure of the observed oscillations is rather complicated. The magnetic field values of some peaks follow a linear dependence on the gate voltage (black dots in Fig. 3c). The B-values of others are almost independent of V_g (red triangles in Fig. 3c). We ascribe the first group of magneto-oscillations with a linear V_g dependence to the Shubnikov – da Haas effect (SdH) in graphene[1]. The dashed lines in Fig. 3c represent the positions of the Landau levels calculated using a capacitance model of the V_g-dependent carrier concentration in graphene and carrier the concentration associated with SdH oscillations[1]:

$$n = \frac{\varepsilon\varepsilon_0}{ed} V_g = \frac{4eB|N|}{h} \quad (1)$$

where $\varepsilon = 3.9$ and $d = 300$ nm are the dielectric constant and thickness of the SiO_2 layer respectively, and N is Landau level index. The second group of oscillations (red triangles in Fig. 3c) are indicated by red arrows in Fig. 3a. They are periodic in $1/B$ and most pronounced for $V_g > 30$ V. Their period is essentially independent of V_g, and hence of the carrier density (Fig. 3c). These oscillations persist over a wide range of temperatures up to about 350 K (80 °C), as shown in Fig. 2d. These observations indicate that they cannot be due to the Shubnikov-de Haas effect, which is dependent on the carrier concentration Eq. (1) and requires that the thermal energy k_BT is small compared to the Landau level separation and the Fermi energy. The field-dependence of V_g-independent oscillations can be fitted empirically to an exponentially damped cosine function of the form

$$\Delta R = R_0 \exp\left(\frac{-\gamma B_f}{B}\right) \cos\left(\frac{2\pi B_f}{B} + \varphi\right) \quad (2)$$

where $B_f = 24$ T determines the characteristic period, $\gamma \approx 1.0$ is the damping term and $\varphi \approx \pi/10$ is a phase factor, see Supplementary Note 2 for details of the fit.

Discussion

We now consider the physical mechanism responsible for the V_g-independent magneto-oscillations. Their characteristic frequency $B_f = 24$ T is quite similar to the condition for the magnetophonon resonance effect in graphene[25,26]. Magnetophonon resonance appears as a series of maxima (or minima) in the magnetoresistance when the condition $N\hbar\omega_c = \hbar\omega_p$ is satisfied. Here, N is an integer and $\hbar\omega_p$ is the energy of the phonon involved in the scattering process, typically a weakly-dispersed longitudinal optic-mode phonon[25,26]. These well-established phenomena are not responsible

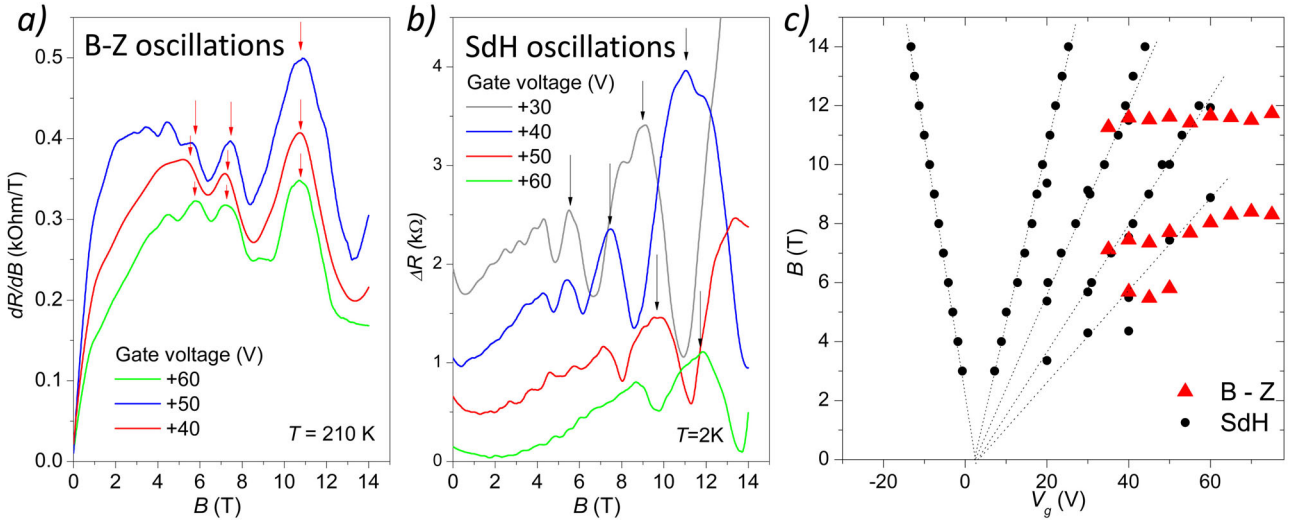

Fig. 3 | Shubnikov-de Haas and Brown-Zak oscillations. a Differential magnetoresistance, dR/dB, of the MBE graphene device at $T = 210$ K for a range of gate voltages, V_g, showing Brown-Zak (B-Z) magneto-oscillations (peaks are indicated by the red arrows). **b** Magnetoresistance ($\Delta R = R(B)-R(B=0)$) at $T = 2$ K showing Shubnikov-de Haas (SdH) oscillations (indicated by the black arrows). The plots are offset for clarity. **c** Fan-diagram showing positions of the SdH oscillations (black circles) and of B-Z oscillations (red triangles). Dashed lines represent Landau levels.

for the V_g-independent magneto-oscillations observed in our graphene-hBN heterostructures. Instead, they arise from magneto-oscillations associated with the Hofstadter butterfly band structure[20,21]. This phenomenon was recently observed in crystallographically-aligned layers of exfoliated graphene on hBN and has been given the name Brown-Zak[22,23] magneto-oscillations, recently reported in hBN encapsulated exfoliated graphene with high electron mobility $\mu > 10{,}000$ cm^2/Vs[27–29]. The frequency B_f is related to the area, A, of the unit cell of the moiré superlattice, $B_f = h/eA$. Our experimental value $B_f = 24$ T implies a moiré periodicity $a = 14$ nm consistent with our AFM images (Fig. 1f).

Interestingly, in our samples we observe Brown-Zak oscillations in graphene layers with relatively low mobility $\mu \sim 1000$ cm^2/Vs, where no Brown-Zak oscillations have been previously reported to our knowledge. We ascribe this behaviour to the high purity of our MBE-grown graphene. The doping level in our graphene layer is $N_{imp} < 10^{11}$ cm^{-2} (Fig. 1c, d). Scattering by ionised impurities is regarded as a major mobility-limiting mechanisms for graphene layers such as CVD graphene on SiO_2/Si[30,31]. However, the impurity density required to reduce electron mobility to $\mu < 1000$ cm^2/Vs, is $N_{imp} > 5 \times 10^{12}$ cm^{-2} (corresponding to $V_g \approx +70$ V)[30], which is about 2 orders of magnitude higher than carrier concentration measured at $V_g = 0$, $p = 8.2 \times 10^{10}$ cm^{-2} (Fig. 1c). Other scattering mechanisms: phonons[32], surface corrugations[33], sample edges[34], are usually ignored in devices with such a low mobility as their mobility limits are typically $\mu > 10{,}000$ cm^2/Vs[32–34]. The presented device does not have the hBN capping layer used in some ultrahigh mobility ($\mu > 100{,}000$ cm^2/Vs) exfoliated[35] and CVD[4] hBN/graphene/hBN FETs. Without a top hBN layer, FETs made using high-purity ($p/n < 10^{11}$ cm^{-2}) graphene typically demonstrate mobilities much higher than 1000 cm^2/Vs[24,36], suggesting that mobility of our HT-MBE graphene is limited by the growth-related processes rather than post-growth contamination.

It is possible that the scattering mechanism responsible for $\mu \approx 1000$ cm^2/Vs in our HT-MBE-grown graphene/hBN layer is related to the very high level of strain generated during HT-MBE growth. Previously, in similar HT-MBE graphene-hBN heterostructure we reported that the strain can be > 1%[11,12]. The moiré pattern periodicity of 14 nm (Fig. 1f) and Raman spectrum (Fig. 1b) indicate that this strain is largely relaxed in the device investigated here[12]. The Raman spectrum (Fig. 1b) also differs significantly from the Raman spectra of high mobility (> 100,000 cm^2/Vs) graphene layers[4,35]. The relative intensity of the 2D and G peaks I(2D)/I(G) ≈ 1.7 is similar to the ratio observed in high-quality monolayer graphene. However, the full width at half maximum of the 2D peak is large, 54 cm^{-1}, compared to that (< 20 cm^{-1}) reported for high mobility graphene[4,35]. The wide 2D peak may arise from small, nanometre-scale strain[35], which can affect electron mobility in high quality hBN/graphene[4]. Also, we observe an additional peak at 1350 cm^{-1} (D_{ag} peak in Fig. 1c) associated with graphene aggregates on the HT-MBE graphene surface[11,12]. These aggregates are visible as small bright spots in the AFM image of the device (Fig. 1e). Previously, we suggested that the aggregates provide pinning sites that maintain the strain in the epitaxial graphene when cooling down from the high growth temperatures[12]; however, their role in electron transport and their effect on graphene mobility have not been studied yet.

The specific growth conditions responsible for the low carrier concentration and mobility in MBE graphene (ultrahigh growth temperature (1500°C), post growth relaxation processes[11,12]) cannot be achieved in other types of epitaxial or exfoliated graphene making it difficult to compare the mobility-limiting mechanics in our HT-MBE FET with other graphene FETs. Further theoretical and experimental studies are required to reveal details of the electron transport in the HT-MBE graphene as it can significantly limit its applicability in high mobility electronic applications.

Methods

MBE growth of graphene on hBN

Our MBE graphene layers are grown at high substrate temperatures (1500°C) on hBN flakes which are exfoliated from high-temperature- and high-pressure-grown bulk hBN crystals and mounted on a sapphire substrate. The samples are grown in a custom-designed Veeco GENXplor MBE system (base pressure ~10^{-10} Torr) that is described in our earlier publications[11–13]. The carbon flux incident on the hBN is generated by Joule-heating a high-purity graphite filament for ~5 h in order to form a continuous graphene monolayer on hBN. Details of the growth process are given in the Supplementary Note 3 and our prior publications[11,12].

Device fabrication

Following MBE growth, a single graphene-hBN flake was transferred using a micromanipulator from the sapphire surface to the Si/SiO_2 wafer (300 nm SiO_2). The graphene was etched using reactive ion etching (RIE) to define the device geometry and contacts were fabricated using electron beam lithography. Additional details of the device fabrication process are given in the Supplementary Note 4.

AFM imaging

AFM imaging of the MBE graphene devices was performed in ambient conditions with an Asylum Research Cypher-S AFM in amplitude-modulated tapping mode (AC-mode) using Budget Sensors Al75-G cantilevers tuned to 5% below the free-air amplitude at resonance. All AFM images were analysed using the Gwyddion[37] software package.

Transport measurements

Transport and magneto-transport measurements were conducted in helium atmosphere using Keithley-2400 source-meters and Keithley-2010 multimeters. Helium filled magneto-cryostat with maximum magnetic field of 14 T (Cryogenic Ltd.) was used for measurements in the temperature range 2 K < T < 210 K (Fig. 3). A cryogen free magnet with open 50 mm bore and maximum magnetic field of 18 T (Cryogenic Ltd.) was used for the measurements in the temperature range 228 K < T < 314 K (Fig. 2d).

Conclusions

We have measured the electrical transport properties of field effect transistors fabricated by growing a monolayer of graphene on hBN by high temperature MBE. Its unique properties include ultra-high purity (doping < 10^{11} cm^{-2}), relatively low and temperature-independent mobility ($\mu \approx 1000$ cm^2/Vs), and a perfect match of the hBN and graphene lattices. We found that high (1500 °C) growth temperature and the orientational alignment of the graphene and hBN lattices give rise to a number of interesting phenomena, such as a moiré-fringed hexagonal superlattice pattern which transforms its electronic band structure into the form of the "Hofstadter butterfly". The reported low (~1000 cm^2/Vs) carrier mobility in such a clean (doping level < 10^{11} cm^{-2}) graphene layers is related to the HT-MBE growth and post-growth relaxation processes. In strong magnetic fields we observe Brown-Zak oscillations above room temperature previously reported only in high mobility graphene. Our transistors based on HT-MBE graphene/hBN heterostructures are a useful platform for observation of room temperature quantum effects and future device applications.

Data availability

All data used in this work are available from the correspondent author on reasonable request.

Received: 7 May 2024; Accepted: 5 September 2024;
Published online: 14 September 2024

References

1. Novoselov, K. S. et al. Electric field effect in atomically thin carbon films. *Science* **306**, 666–669 (2004).
2. Bolotin, K. I. et al. Ultrahigh electron mobility in suspended graphene. *Solid State Comm.* **146**, 351–355 (2008).
3. Mayorov, A. S. et al. Micrometer-Scale Ballistic Transport in Encapsulated Graphene at Room Temperature. *Nano Lett.* **11**, 2396–2399 (2011).
4. Banszerus, L. et al. Ultrahigh-mobility graphene devices from chemical vapor deposition on reusable copper. *Sci. Adv.* **1**, e1500222 (2015).
5. Yankowitz, M. et al. Emergence of superlattice Dirac points in graphene on hexagonal boron nitride. *Nat. Phys.* **8**, 382–386 (2012).
6. Ponomarenko, L. A. et al. Cloning of Dirac fermions in graphene superlattices. *Nature* **497**, 594–597 (2013).
7. Wallbank, J. et al. Generic miniband structure of graphene on a hexagonal substrate. *Phys. Rev. B* **87**, 245408 (2013).
8. Yan, X. et al. Moiré synaptic transistor with room temperature neuromorphic functionality. *Nature* **624**, 551–556 (2023).
9. Taniguchi, T. et al. Synthesis of high-purity boron nitride single crystals under high pressure by using Ba-BN solvent. *J. Cryst. Growth* **303**, 525–529 (2007).
10. Martini, L. et al. Scalable High-Mobility Graphene/hBN Heterostructures. *ACS Appl. Mater. Interfaces* **15**, 37794–37801 (2023).
11. Summerfield, A. et al. Strain-engineered graphene grown on hexagonal boron nitride by molecular beam epitaxy. *Sci. Rep.* **6**, 22440 (2016).
12. Davies, A. et al. Lattice-Matched Epitaxial Graphene Grown on Boron Nitride. *Nano Lett.* **18**, 498–504 (2018).
13. Summerfield, A. et al. Moire-Modulated Conductance of Hexagonal Boron Nitride Tunnel Barriers. *Nano Lett.* **18**, 4241–4246 (2018).
14. Moreau, E. et al. Graphene growth by molecular beam epitaxy on the carbon-face of SiC. *Appl. Phys. Lett.* **97**, 241907 (2010).
15. Xu, Z. et al. Direct growth of hexagonal boron nitride/graphene heterostructures on cobalt foil substrates by plasma-assisted molecular beam epitaxy. *Appl. Phys. Lett.* **109**, 043110 (2016).
16. Plaut, A. S. et al. Exceptionally large migration length of carbon and topographically-facilitated self-limiting molecular beam epitaxial growth of graphene on hexagonal boron nitride. *Carbon* **114**, 579–584 (2017).
17. Geim, A. K. & Grigorieva, I. V. Van der Waals heterostructures. *Nature* **499**, 419–425 (2013).
18. Ferrari, A. C. et al. Science and technology roadmap for graphene, related two-dimensional crystals, and hybrid systems. *Nanoscale* **7**, 4598–4810 (2015).
19. Novoselov, K. S. et al. 2D materials and van der Waals heterostructures. *Science* **363**, 461–474 (2016).
20. Dean, C. R. et al. Hofstadter's butterfly and the fractal quantum Hall effect in moiré superlattices. *Nature* **497**, 598–602 (2013).
21. Hunt, B. et al. Massive Dirac fermions and Hofstadter butterfly in a van der Waals heterostructure. *Science* **340**, 1427–1430 (2013).
22. Brown, E. Bloch electrons in a uniform magnetic field. *Phys. Rev.* **133**, A1038–A1044 (1964).
23. Zak, J. Magnetic translation group. *Phys. Rev.* **134**, A1602–A1606 (1964).
24. Morozov, S. V. et al. Giant Intrinsic Carrier Mobilities in Graphene and Its Bilayer. *Phys. Rev. Lett.* **100**, 016602 (2008).
25. Mori, N. & Ando, T. Magnetophonon resonance in monolayer graphene. *J. Phys. Soc. Jpn.* **80**, 044706 (2011).
26. Wang, C. M. & Luan, X. Y. Surface-optical-phonon–induced magnetophonon resonance in graphene. *Europhys. Lett.* **103**, 37012 (2013).
27. Krishna Kumar, R. et al. High-temperature quantum oscillations caused by recurring Bloch states in graphene superlattices. *Science* **357**, 181–184 (2017).
28. Krishna Kumar, R. et al. High-order fractal states in graphene superlattices". *PNAS* **115**, 5135–5139 (2018).
29. Huber, R. et al. Band conductivity oscillations in a gate-tunable graphene superlattice. *Nat. Comm.* **13**, 2856 (2022).
30. Adam, S. et al. A self-consistent theory for graphene transport. *PNAS* **104**, 18392–18397 (2007).
31. Xuesong Li. et al. Large-Area Synthesis of High-Quality and Uniform Graphene Films on Copper Foils. *Science* **324**, 1312–1314 (2009).
32. Hwang, E. H. & Das Sarma, S. Acoustic phonon scattering limited carrier mobility in two-dimensional extrinsic graphene. *Phys. Rev. B* **77**, 115449 (2008).
33. Wang, L. et al. Mobility Enhancement in Graphene by in situ Reduction of Random Strain Fluctuations. *Phys. Rev. Lett.* **124**, 157701 (2020).
34. Lin, M.-W. et al. Approaching the intrinsic band gap in suspended high-mobility graphene nanoribbons. *Phys. Rev. B* **84**, 125411 (2011).
35. Neumann, C. et al. Raman spectroscopy as probe of nanometre-scale strain variations in graphene. *Nat. Comm.* **6**, 8429 (2015).
36. Chen, B. et al. How good can CVD-grown monolayer graphene be? *Nanoscale* **6**, 15255 (2014).
37. Nečas, D. & Klapetek, P. Gwyddion: an open-source software for SPM data analysis. *Cent. Eur. J. Phys*. **10**, 181 (2012).

Acknowledgements
This work at Nottingham was supported by the Engineering and Physical Sciences Research Council UK (Grants No. EP/L013908/1, No. EP/P019080/1, No. EP/V05323X/1, and No. EP/W035510/1).

Author contributions
O.M. and R.H. did the transport measurements and data analysis. T.Ch. and S.N. grew the material. T.T. and K.W. provided hBN crystals. A.S., C.M. and P.B. processed the material into devices, did AFM measurements and their analysis. A.P. and L.E. participated in discussions and development of the model. All co-authors contributed to the results analysis and model development, co-wrote and approved manuscript submission.

Competing interests
The authors declare no competing interests.

Additional information
Supplementary information The online version contains supplementary material available at https://doi.org/10.1038/s43246-024-00633-x.

Correspondence and requests for materials should be addressed to Oleg Makarovsky.

Peer review information *Communications Materials* thanks the anonymous reviewer(s) for their contribution to the peer review of this work. A peer review file is available. Primary Handling Editors: SangHoon Bae and Aldo Isidori.